Extended Data for

Irreversible Response of the Intertropical Convergence Zone (ITCZ) to CO_2 ramp-up and -down Forcing

Jong-Seong Kug[1†]*, Ji-Hoon Oh[1†], Soon-Il An[2], Sang-Wook Yeh[3], Seung-Ki Min[1], Seok-woo Son[4], Jong-Hoon Kam[1], Yoo-Geun Ham[5], Jongsoo Shin[2]

[1] Division of Environmental Science and Engineering,
Pohang University of Science and Technology (POSTECH), Pohang, South Korea
[2]Department of Atmospheric Sciences, Yonsei University, Seoul, South Korea
[3]Department of Marine Science and Convergent Technology, Hanyang University, ERICA, Ansan, South Koreas
[4]School of Earth and Environmental Sciences, Seoul National University, Seoul, South Korea
[5]Department of Oceanography, Chonnam National University, Gwangju, South Korea
*Corresponding authors. Email: jskug@postech.ac.kr

[†]: These authors contributed equally to this work

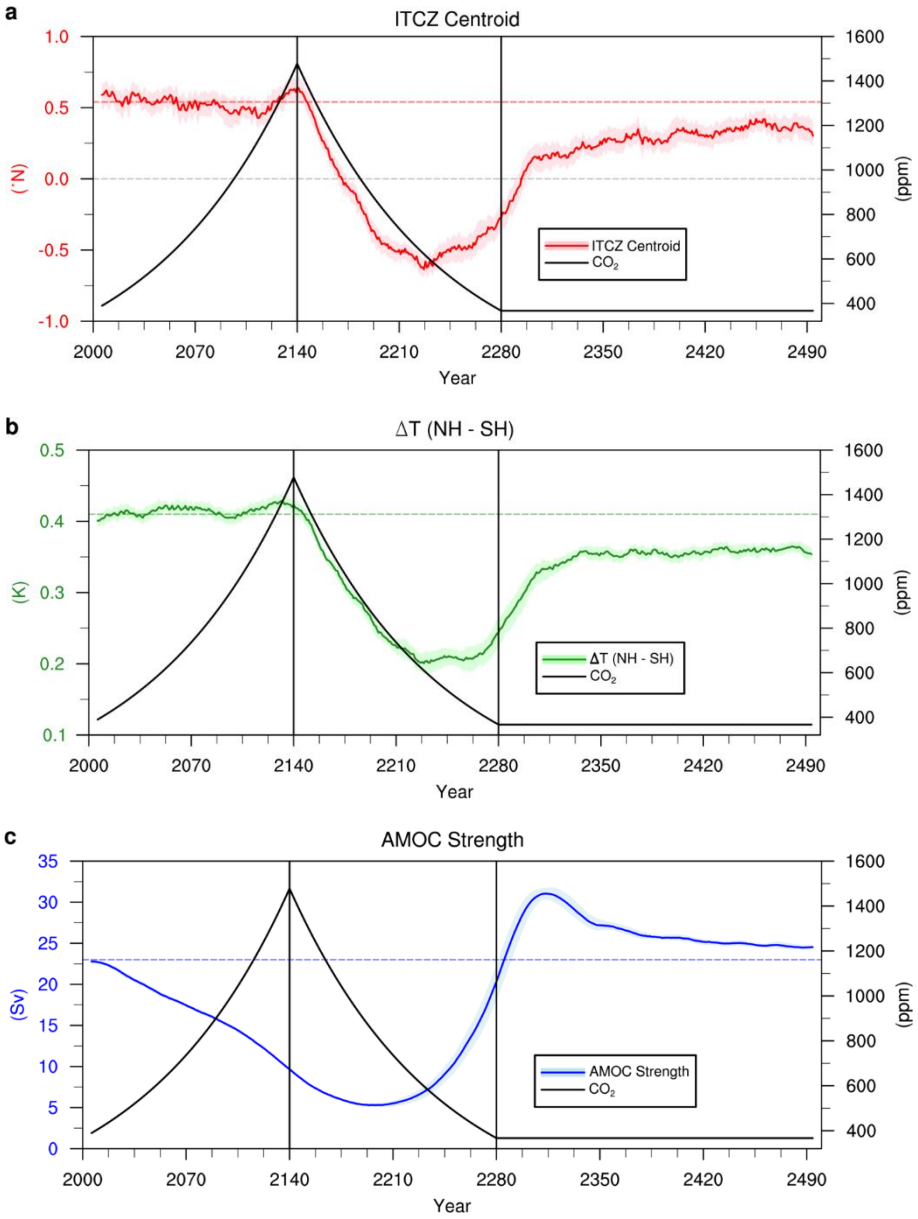

Extended Data Fig. 1 | Time evolution of the ITCZ centroid, interhemispheric temperature gradient and AMOC. Same as indices in Fig. 3b-c, but the time axis is extended Year 2500 (including additional 220 years restoring run). Horizontal dotted lines are long-term climatological values from the long-term present climate simulation (PD). Lines and shadings as in Fig. 1b.

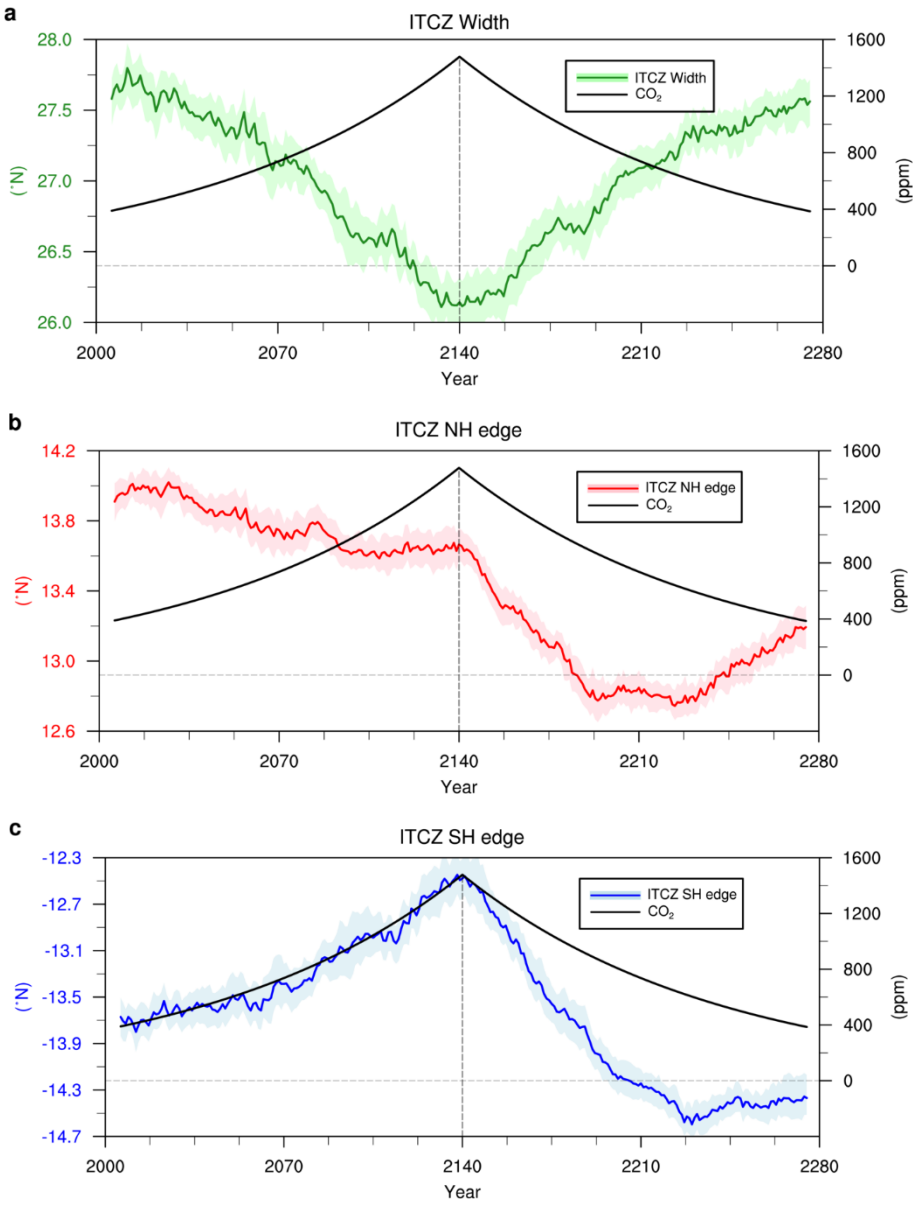

Extended Data Fig. 2 | Time evolution of the ITCZ width, northern and southern edge of the ITCZ. Time series of **a,** ITCZ width, **b,** northern edge and **c,** southern edge of ITCZ. ITCZ edge is defined as the latitude that is changed from a zonal-mean upward motion to a downward motion in the mid-troposphere (700hPa). Lines and shadings as in Fig. 1b.

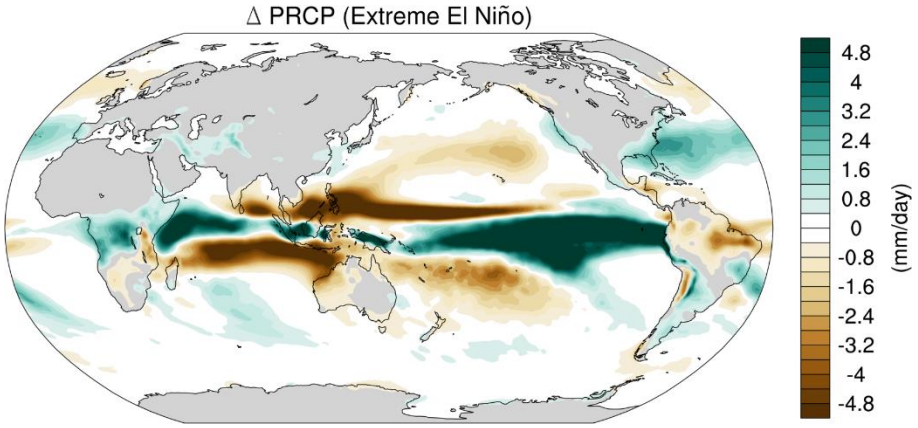

Extended Data Fig. 3 | Precipitation anomalies in the extreme El Niño period. Composite of DJF averaged precipitation anomalies during 82/83, 97/98 and 15/16 El Niño period. The observational precipitation data are the Climate Prediction Merged Analysis of Precipitation (CMAP), which uses a horizontal resolution of 2.5° and covers the period from 1979 to 2018. Note that the seasonal cycle and linear trend is removed from the data.

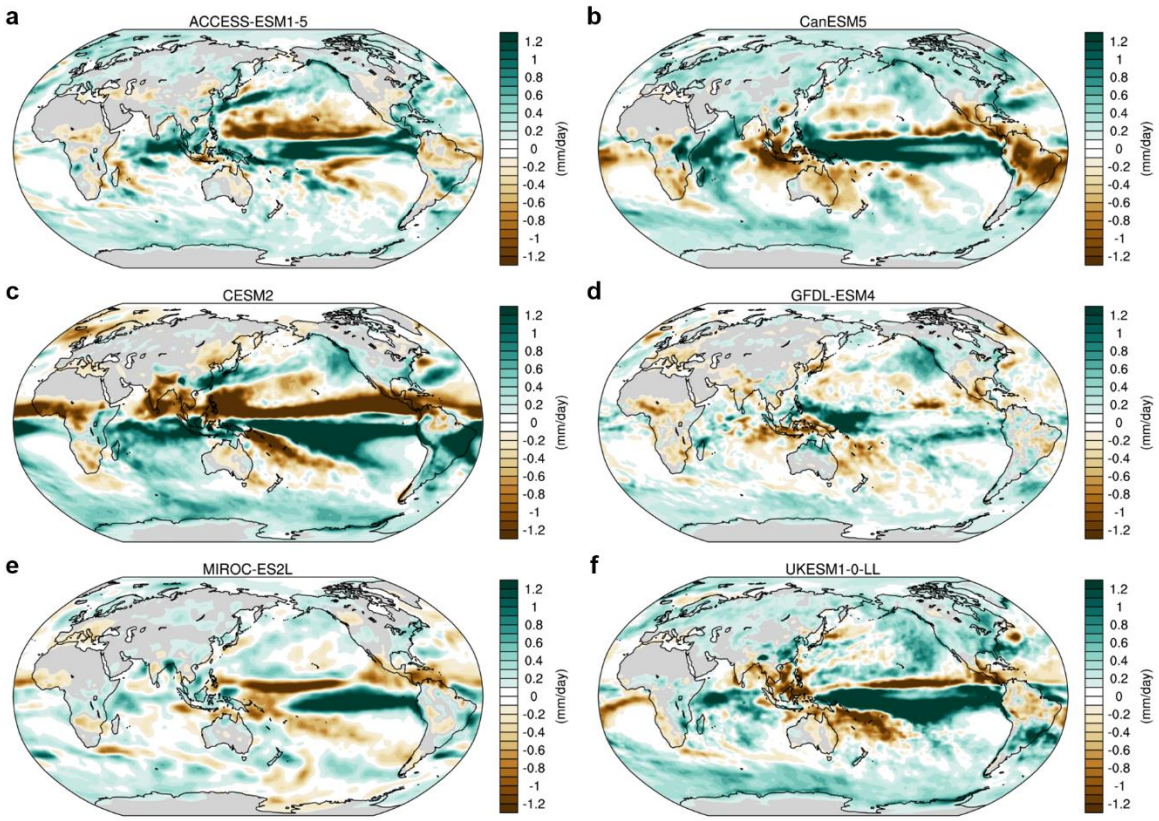

Extended Data Fig. 4 | Changes in global hydrological cycle. Same as Fig. 2c, but the data from the individual models in CMIP6 (ACCESS-ESM1-5, CanESM5, CESM2, GFDL-ESM4, MIROC-ES2L, UKESM1-0-LL).

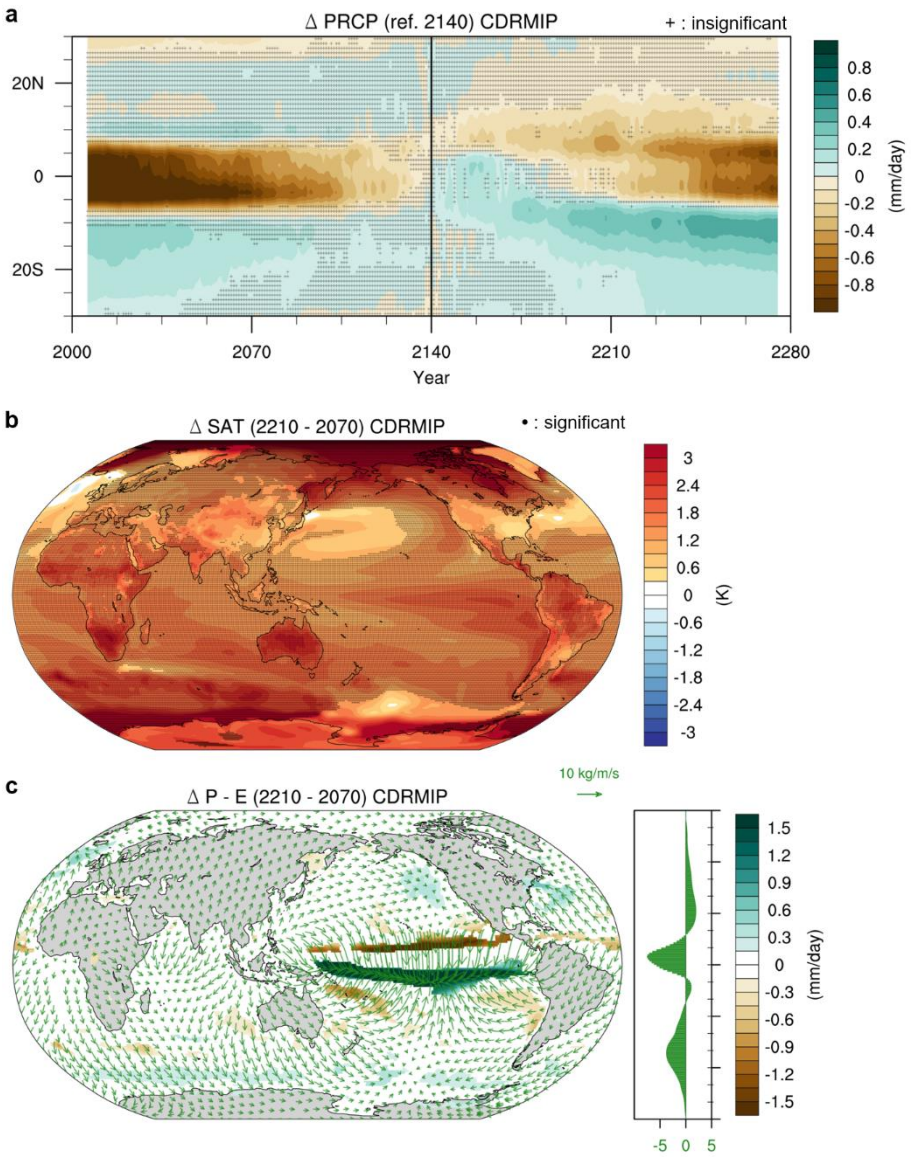

Extended Data Fig. 5 | Changes in global SAT and hydrological cycle. Same as Fig. 2a and d-e, but the data in the multi-model mean from the CMIP6 (ACCESS-ESM1-5, CanESM5, CESM2, GFDL-ESM4, MIROC-ES2L, UKESM1-0-LL).

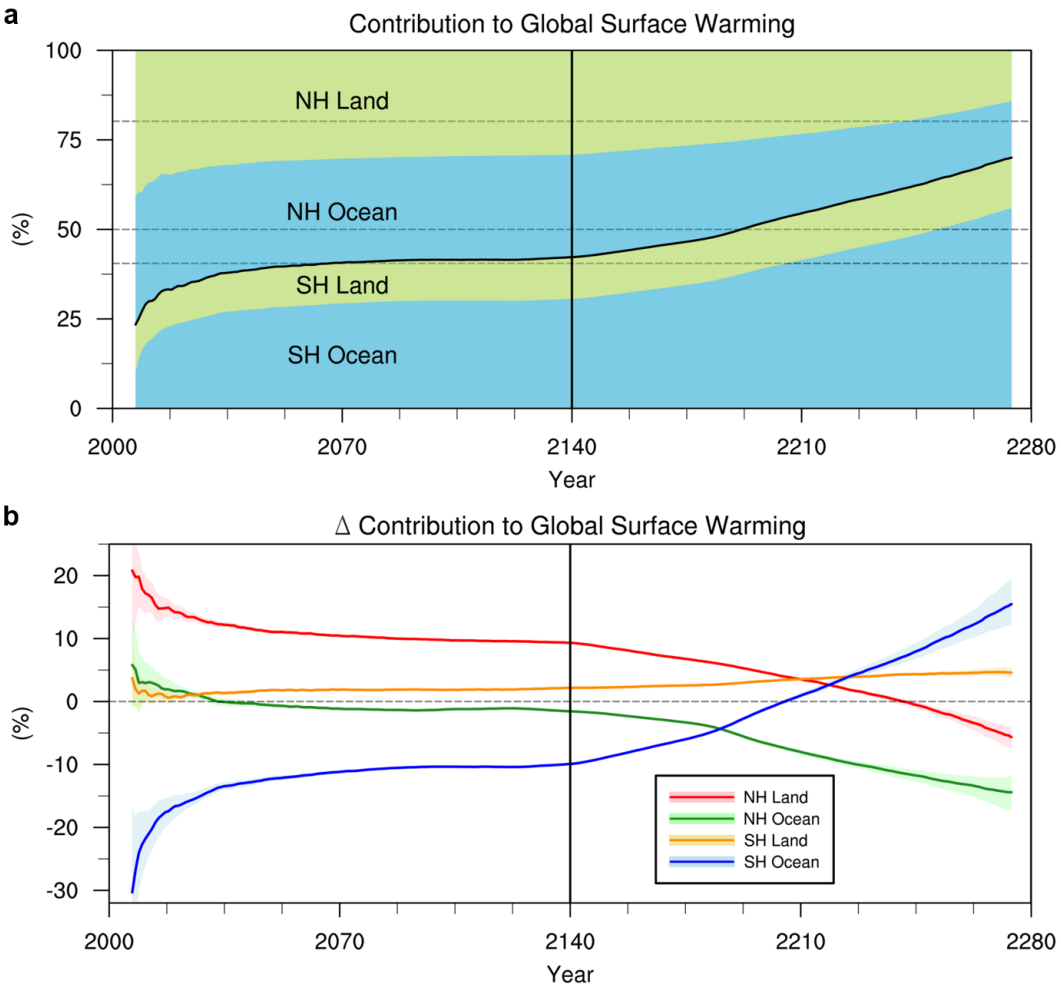

Extended Data Fig. 6 | Land and ocean contribution to global surface warming. a, The percentage of the land and ocean SAT anomalies in the NH and SH for global surface temperature anomaly relative to long-term climatological values of the present climate simulation. Dotted lines represent the ratio of each area to the total earth surface (SH ocean: 40.5%, SH land: 9.5%, NH ocean: 30.2%, NH land: 19.8%). Solid line indicates the boundary of SH land and NH ocean, which represent hemispheric warming contrast. For example, less than 50% of the solid line means that the NH is warmer than the SH. **b,** The deviation of the percentage of each component from the ratio to the total earth surface (deonted in Dotted lines in a). Lines and shadings as in Fig. 1b.

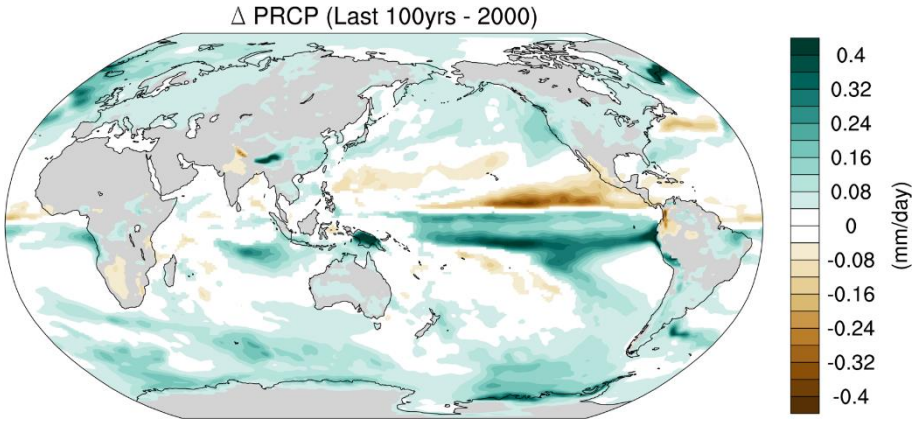

Extended Data Fig. 7 | Precipitation anomalies in the stabilization period. Difference in the precipitation between the mean of 2401 to 2500 years and long-term climatological value at the Year 2000 in the PD. The pattern correlation with Fig. 2b is 0.61. The regions denoted by colors indicate where the responses are significant at the 99% confidence level by using bootstrap test.